Constitutive Equations for Creep and Plasticity of Aluminum Alloys Produced by Powder Metallurgy and Aluminum-Based Metal Matrix Composites

E. EVANGELISTA and S. SPIGARELLI

The constitutive relationships between stress, strain rate, and temperature were analyzed to obtain a unified description of creep and plasticity of aluminum alloys produced by powder metallurgy and of aluminum-based metal-matrix composites. As both classes of materials are characterized by the existence of a threshold stress (σ_0), a unified description of creep (low strain-rate regime) and plasticity (high strain-rate regime) was obtained by substituting the conventional power-law equation with the sinh relationship, where the applied stress is replaced by the difference between the applied stress and a threshold stress. The stress exponent was $n = 3$ or 5, and the activation energy was equivalent to the activation energy for self-diffusion or to the activation energy for diffusion of solute elements in the matrix. The model was applied to an unreinforced alloy (2014PM) and a composite (6061 + 20 pct Al_2O_3) tested in tension (under constant load) or torsion (at constant strain rate) in the temperature range between 300 °C and 500 °C. The results were compared with data available in the literature.

I. INTRODUCTION

THE hot workability of aluminum and its alloys[1–17] has been extensively analyzed in the last decades. These studies have investigated, in particular, the dependence on temperature and strain rate of flow stress and ductility and have correlated these results with the microstructural features typical of these materials. Whereas the majority of these studies have analyzed materials produced by ingot metallurgy, others have also addressed the high-temperature formability of alloys produced by powder metallurgy (PM).[6,11,16]

As aluminum alloys generally have good formability but relatively low strength, the development of aluminum-matrix composites reinforced by ceramic particulate has been one of the main innovations in light-weight materials.[18] Particle-reinforced light alloys, with their comparatively low cost and high modulus, low density, and wear resistance, are now easily available commercially. However, one of the main problems that still needs addressing before discontinuously reinforced particulate composites can be introduced into mass production is their poor ductility during high-temperature forming. The main objective in studying the hot formability of these materials, be they produced by solidification into billets or by PM, is the determination of a proper processing window, *i.e.*, the combination of strain rate and temperature permitting to form defect-free secondary products. Two different approaches have been adopted to this end; one is formally equivalent to that conventionally used to analyze the formability of simple alloys and is based on the calculation of a constitutive equation, *i.e.*, the relationship correlating strain rate ($\dot{\varepsilon}$), temperature (T), and flow stress (σ).[19–25] The second approach is based on the dynamic material model,[26–32] which analyses the energy dissipation efficiency $\eta = 2\ m/[1 + m]$, where $m = \partial \log \sigma / \partial \log \dot{\varepsilon}$, calculated at constant temperature for a given strain. The efficiency of power dissipation is, thus, mapped as a function of temperature and strain rate, and the processing window is selected using the map as the basis.

The situation is further complicated by the fact that the low strain-rate plasticity (*i.e.*, creep) of the same or similar materials is frequently analyzed using a completely different approach, *i.e.*, different forms of constitutive equation.[33–61]

The aim of this study was to obtain a unified description of plasticity using a single constitutive equation to determine the processing window of Al-based composites and complex Al alloys.

II. HIGH STRAIN-RATE PLASTICITY

The design calculation of the forces and power required for forming processes is based on the estimation of the mean values of strain and strain rate and of the corresponding values of flow stress developed during deformation over a range of temperatures. Data are usually obtained by means of compression or torsion tests. Compression tests are reliable if an appropriate lubricant is used to prevent barreling; however, in axisymmetric compression maximum deformation cannot exceed unity. Figure 1 plots an example of true-stress *vs* strain curves obtained by testing in compression a 2618 + 20 pct Al_2O_3 composite after heat treatment at 480 °C for 30 minutes.[62] In the temperature range between 450 °C and 500 °C, after an initial region of strain hardening, the stress remains constant with increasing strain. Only at 350 °C is a moderate peak in the curves observed.

Torsion testing provides larger strains, since in this case flow instability does not occur; however, this kind of test is characterized by a linear gradient of strain and strain rate from the center to the surface of the specimen. Torque (M)

E. EVANGELISTA, Professor, and S. SPIGARELLI, Researcher, are with the Department of Mechanics, INFM/University of Ancona, Italy.

This article is based on a presentation made in the workshop entitled "Mechanisms of Elevated Temperature Plasticity and Fracture," which was held June 27–29, 2001, in San Diego, CA, concurrent with the 2001 Joint Applied Mechanics and Materials Summer Conference. The workshop was sponsored by Basic Energy Sciences of the United States Department of Energy.

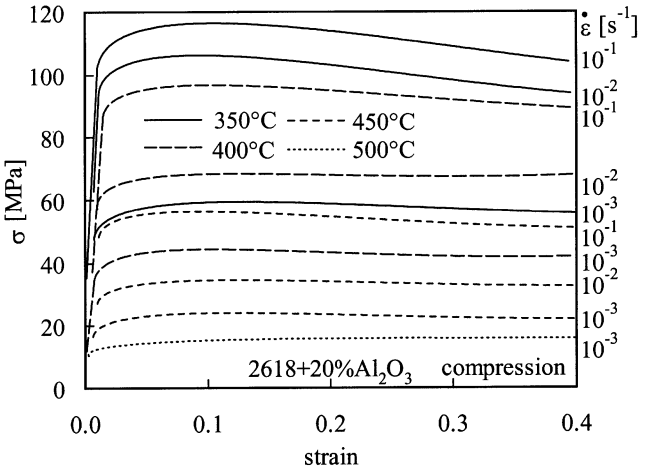

Fig. 1—Stress *vs* strain curves obtained by testing the 2618 + 20 pct Al_2O_3 composite in compression in as-extruded condition.[62]

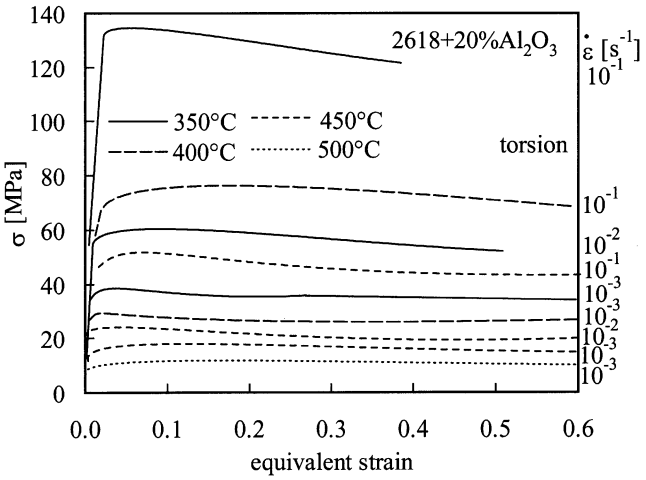

Fig. 2—Equivalent stress *vs* equivalent strain curves obtained by testing the 2618 + 20 pct Al_2O_3 composite in torsion; the material was heat treated at 480 °C for 30 min prior to testing.[62]

and number of revolutions (N) are usually converted into equivalent stress and equivalent strain by means of the well-known relationships:

$$\varepsilon = \frac{2\pi NR}{\sqrt{3}L} \qquad [1]$$

$$\sigma = \frac{\sqrt{3}M}{2\pi R^3}(3 + \hat{m} + \hat{n}) \qquad [2]$$

where R is the sample radius, $\hat{m} = \partial \log M/\partial \log \dot{R}$ and $\hat{n} = \partial \log N/\partial \log R$. In steady state or at the peak, $\hat{n} = 0$; the value of $\hat{m}$ is also usually taken equal to zero. Figure 2 plots the equivalent-stress *vs* equivalent-strain curves obtained by testing the 2618 + 20 pct Al_2O_3 composite in as-extruded condition.[62] When the same material is tested in the same initial condition (as in the case of the 6061 + 20 pct Al_2O_3 composite, tested in compression and torsion in the as-extruded state),[63,64] the effective-stress *vs* effective-strain curve at the same temperature and strain rate are substantially the same in both compression and torsion.[1]

As shown in Figures 1 and 2, when deformation temperature is raised or the strain rate is reduced, the rate of strain hardening, the steady-state stress, or the peak stress decrease. In metals and alloys,[1,2] the stress in steady state or at a fixed value of strain is normally related to temperature and strain rate by one of the following equations:

$$\dot{\varepsilon} = A\sigma^n \exp(-Q/RT) \qquad [3]$$

$$\dot{\varepsilon} = A(\sinh \alpha\sigma)^{n'} \exp(-Q/RT) \qquad [4]$$

where A and α are constants, n and n' are the stress exponents, R is the gas constant, and Q is the activation energy of the rate-controlling process. While Eq. [4] is of general validity (*i.e.*, for strain rates ranging from 10 to 10^{-8} s^{-1}),[1] the power-law Eq. [3] is useful at lower stresses (*i.e.*, for $\alpha\sigma < 0.8$). A plot of log ($\dot{\varepsilon}$) *vs* log (σ) (Eq. [3]) or *vs* log (sinh $\alpha\sigma$) (Eq. [4]) should result in a family of isothermal straight lines of slope n or n', respectively. When the strain rate is plotted in temperature-normalized form, *i.e.*, as $Z = \dot{\varepsilon} \exp(Q/RT)$, all the isothermal curves should collapse on a single line. Yet, in the case of Eq. [3], when the strain rate exceeds a limit—calculated by some authors[65] as $\dot{\varepsilon}/D = 10^{13}$ m^{-2}, D being the appropriate diffusion coefficient, power-law breakdown (PLB) results in a progressive increase in the slope of the log ($\dot{\varepsilon}$) *vs* log (σ) curves.

In this respect, an obvious disadvantage with the use of Eq. [4] is that, even for alloys with similar Q values, a direct comparison between the log ($\dot{\varepsilon}$) *vs* log (sinh $\alpha\sigma$) plots for different materials is misleading, since α may be different.

The high-temperature plasticity of a number of Al alloys has been studied extensively in the past by plotting steady-state stress or peak stress as a function of strain rate using Eq. [4].[1–17] In the present study, the flow stress at the peak or at a given strain just before or after the peak (normally these values do not differ appreciably) for the Al-based composite and the unreinforced alloy produced by PM described previously, was instead directly plotted as a function of strain rate in Figures 3(a) (2618, as-extruded, torsion)[62] and (b) (2618 + 20 pct Al_2O_3, as-extruded, compression),[62] 4(a) (6061 + 20 pct Al_2O_3 as-extruded, torsion).[63] and (b) (6061 + 20 pct Al_2O_3, as-extruded, compression),[64] and 5 (2014PM, stabilized for 24 hours at the testing temperature, torsion).[66] For comparison purposes, Figure 6 plots an example of the data obtained by other authors in compression.[28,67,68]

The analysis of Figures 3 through 6 provides some generalities on the phenomenology of high strain-rate plasticity in Al-based composites: in particular, for materials tested in the same initial state, the use of Eq. [3] results in similar values of the stress exponent, which usually decreases when temperature increases (n = 5 to 8 for 6061 and 2618 alloys and their composites). In addition, PLB is not so evident as could be expected, since the log ($\dot{\varepsilon}$) *vs* log (σ) curves are linear up to very high strain rates for both compression and torsion data, even though the n values are larger than the theoretical ones (n = 3 to 5).[69,70] In general, the activation energy is close to, but invariably slightly higher than, the activation energy for self-diffusion in Al (143 kJ mol^{-1}).[69]

III. LOW-STRAIN RATE PLASTICITY (CREEP)

The minimum or steady-state creep rate for Al-based composites or Al alloys produced by PM has been described on the basis of the same assumption as used to analyze high strain-rate plasticity, *i.e.*, that in steady state or, by extension,

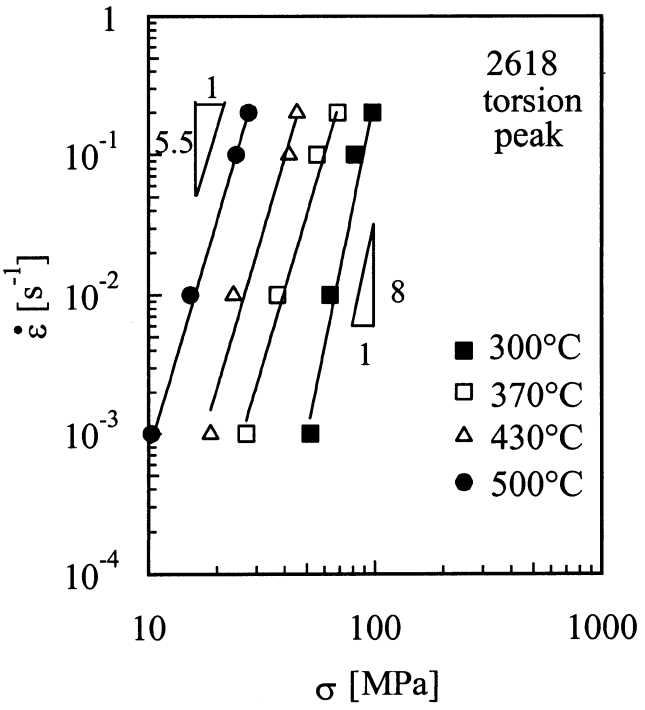

(*a*)

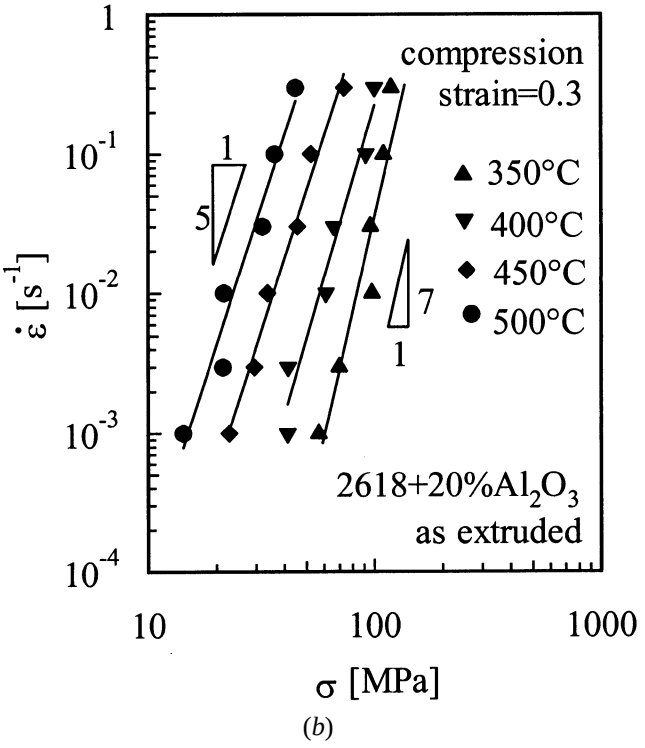

(*b*)

Fig. 3—(*a*) Equivalent stress at peak *vs* strain rate obtained by testing the 2618 alloy in torsion; the material was tested in the as-extruded state.[62] (*b*) Stress at $\varepsilon = 0.3$ *vs* strain rate obtained by testing the 2618 + 20 pct Al_2O_3 composite in compression; the material was tested in the as-extruded condition.[62]

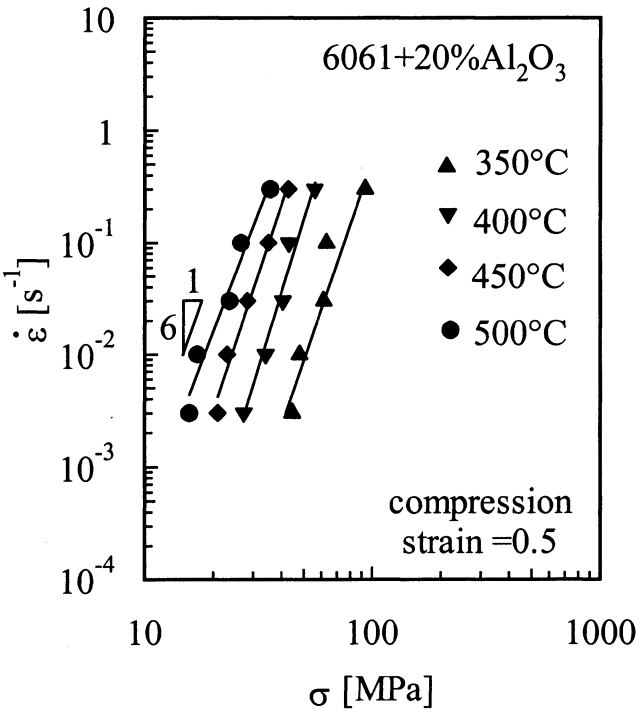

(*a*)

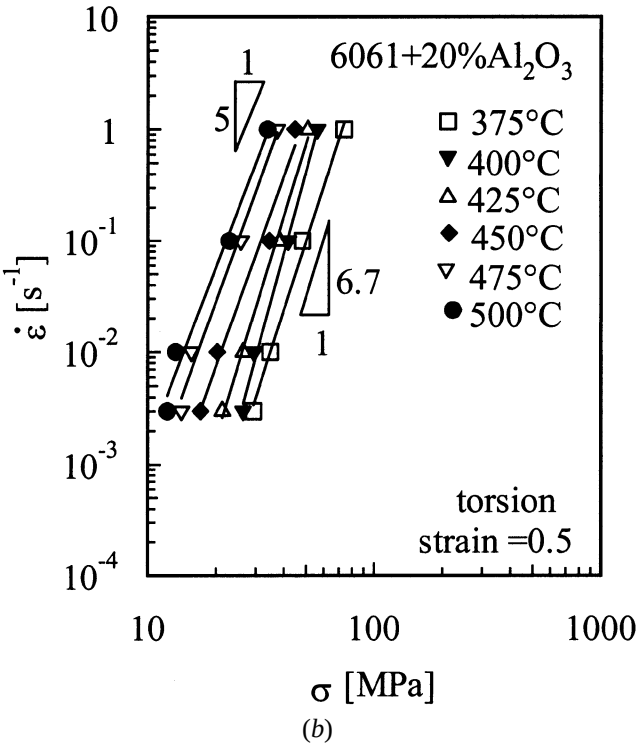

(*b*)

Fig. 4—(*a*) Stress at $\varepsilon = 0.5$ *vs* strain rate obtained by testing the 6061 + 20 pct Al_2O_3 composite in compression; the material was tested in the as-extruded condition.[63] (*b*) Equivalent stress at $\varepsilon = 0.5$ *vs* strain rate obtained by testing the 6061 + 20 pct Al_2O_3 composite in torsion; the material was tested in the as-extruded condition.[64]

in the minimum creep-rate range, the microstructures of specimens tested at different temperatures appear approximately identical for a fixed stress, or, more correctly, for a fixed modulus-compensated stress (σ/G).[70]

In pure metals and in simple alloys, the phenomenological relationship between steady-state (or minimum) creep rate and applied stress, thus, takes the form

$$\dot{\varepsilon}_m = A_0 \frac{DG\mathbf{b}}{\mathrm{k}T} \left(\frac{\sigma}{G}\right)^n \qquad [5]$$

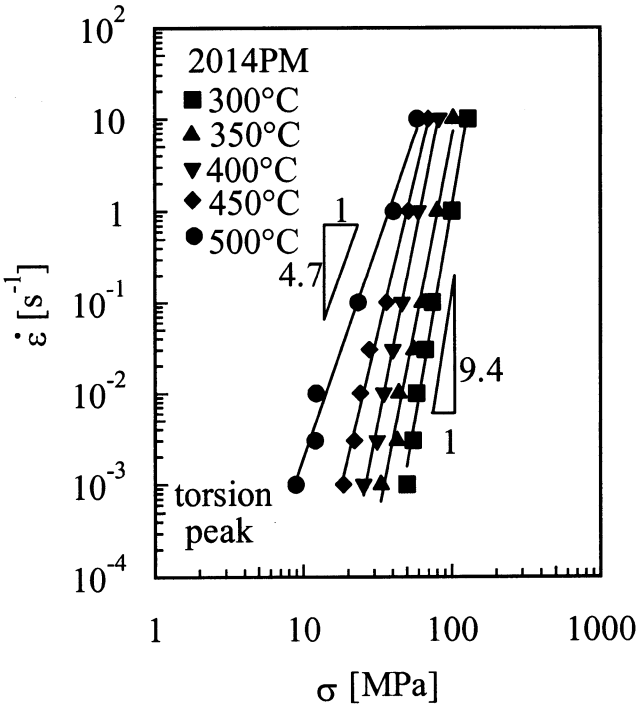

Fig. 5—Equivalent stress at peak *vs* strain rate obtained by testing the 2024PM alloy in torsion.[66]

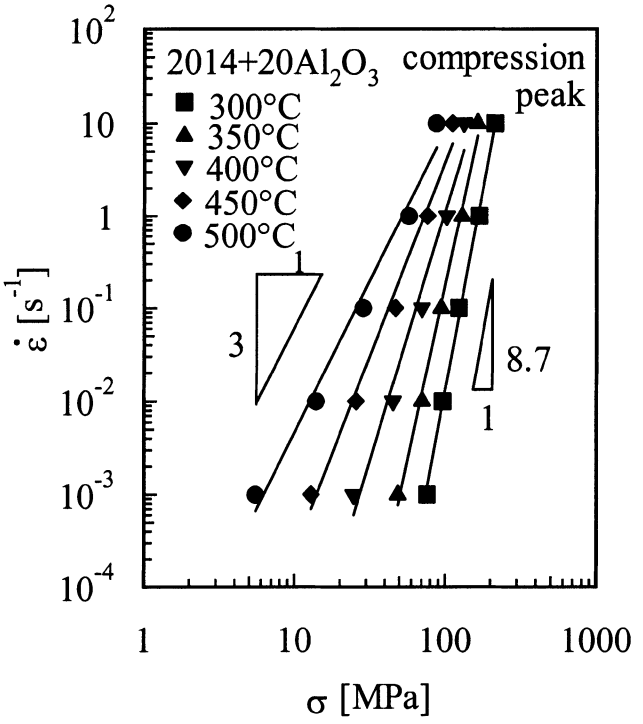

Fig. 6—Stress at peak *vs* strain rate obtained by testing the 2014 + 20 pct Al_2O_3 alloy in compression.[28,68]

where D is the appropriate diffusion coefficient ($= D_0 \exp(-Q/RT)$), D_0 being a frequency factor, and Q the activation energy for creep), **b** is the Burgers' vector, k is the Boltzmann constant, n is the stress exponent, and A_0 is a dimensionless constant. By contrast, a hyperbolic sine equation[70] is used to describe transition from power law to PLB (which, in the range of strain rate typical of creep, is normally observed only when testing temperature is low), *i.e.*,

$$\dot{\varepsilon}_m = A' \exp\left(\frac{-Q}{RT}\right)\left(\sinh\left(\frac{\sigma}{G}\right)\right)^{n'} \qquad [6]$$

It is easy to observe that Eq. [5] is similar to Eq. [3], and that Eq. [6] is substantially equivalent to Eq. [4]; this is not surprising since, although high- and low-strain rate regimes are usually investigated using different procedures and with different aims, both are based on similar microstructural mechanisms (mainly recovery for materials that do not exhibit extensive dynamic recrystallization).

In the last two decades, numerous investigations have been conducted to determine the high-temperature creep response of several aluminum-based discontinuously reinforced composites.[33–61] For instance, the creep properties of 6XXX alloys[60,71] and their composites,[34–36,39,54–56,59,60] produced by powder metallurgy[34–36,60,71] or ingot casting[34–36,39,54–56] and reinforced with SiC or Al_2O_3, have been investigated by means of constant-load tensile tests. Other investigations have addressed the creep response of pure Al reinforced with SiC particles[44,51] or of composites with matrices of the 7XXX[57] and 2XXX groups.[42,43,49,72]

In the majority of cases, when the minimum creep rate is represented in logarithmic scale as a function of applied stress, the slope of the resulting curve increases when applied stress decreases. This behavior has commonly been associated with the presence of a threshold stress (σ_0)[61] that decreases with increasing temperature. A thresholdlike behavior has been observed not only in composites but also in unreinforced alloys produced by PM.[60,71] The threshold stress represents a limiting value below which creep should not occur and is generated by the presence of fine particles (precipitates or dispersoids) that obstruct dislocation mobility. When the applied stress is substituted by the effective stress, *i.e.*, by the difference between the applied stress and threshold stress, the value of the true-stress exponent, n, is close to the theoretical values $n = 4$ to 5 for climb-controlled creep or $n = 3$ for creep controlled in viscous glide. The true activation energy for creep is close to the activation energy for self-diffusion in Al or to the activation energy for interdiffusion of the solute atoms in the case of dilute solid-solution alloys, where creep is controlled by viscous glide. Moreover, it has been shown that the same composite can exhibit one behavior with $n = 3$ in a certain stress regime, and a different behavior with $n = 4$ to 5 in a higher range of applied stress. The transition between the different regimes can reasonably be predicted by suitable calculations.[73] On these bases, Eq. [5] should be modified into

$$\varepsilon_m = A\,\frac{DG\mathbf{b}}{kT}\left(\frac{\sigma - \sigma_0}{G}\right)^n \qquad [7]$$

Figure 7 shows the typical behavior of an Al alloy produced by powder metallurgy and of Al-matrix composites. In these examples, when the temperature-normalized strain rate is plotted as a function of modulus-compensated effective stress (Figure 8), all data fall on the same line of slope close to 4 to 5.[72]

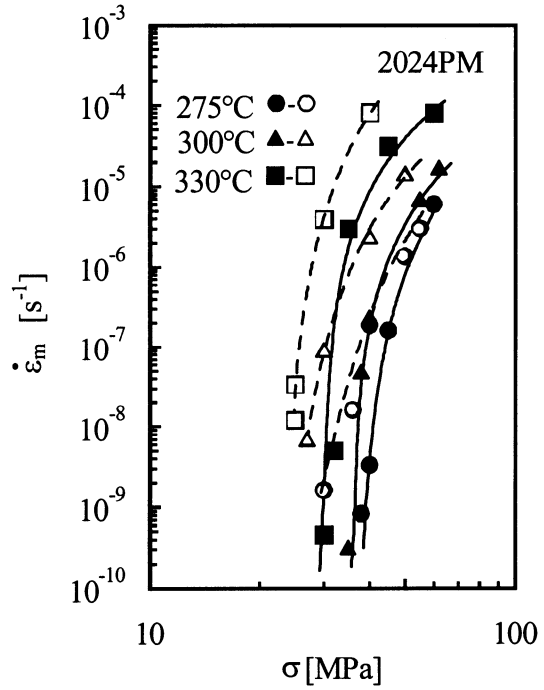

Fig. 7—Minimum creep rate as a function of applied stress for the 2024 alloy (open symbols) and the 2024 + 15 pct SiC composite (solid symbols) produced by powder metallurgy.[72]

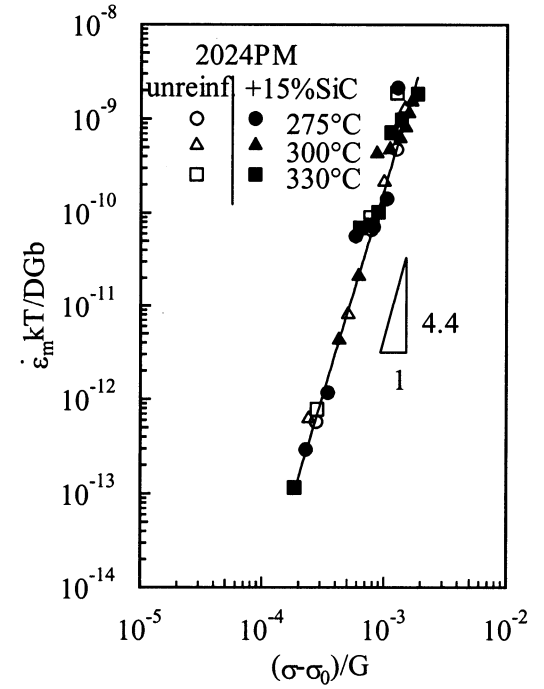

Fig. 8—Temperature-normalized creep rate as a function of modulus-compensated effective stress for the 2024PM and 2024PM + 15 pct SiC.[72]

IV. A UNIFIED APPROACH TO THE PLASTICITY OF MATERIALS EXHIBITING A THRESHOLD STRESS

The preceding discussion indicates that high-temperature plasticity of Al-based composites is conventionally described by an equation in the form:

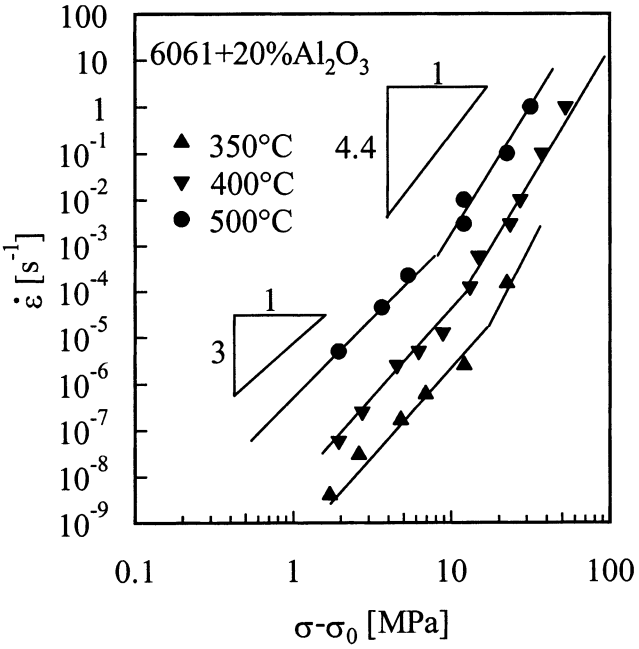

Fig. 9—Minimum creep rate as a function of effective stress for the 6061 + 20 pct Al_2O_3 tested in torsion[64] and shear.[54]

$$\dot{\varepsilon} \propto (\sinh \alpha\sigma)^{n'} \exp(-Q/RT) \qquad [4a]$$

whereas creep data are described by means of the relationship

$$\dot{\varepsilon}_m \propto \left(\frac{\sigma - \sigma_0}{G}\right)^n \exp(-Q/RT) \qquad [7a]$$

These two approaches can easily be reconciled by simply assuming that for the same material creep and high strain-rate plasticity are two aspects of the same phenomena, described by a simple equation in the form

$$\dot{\varepsilon}_m \propto \left(\sinh \alpha_0 \frac{\sigma - \sigma_0}{G}\right)^n \exp(-Q/RT) \qquad [8]$$

where α_0 is a dimensionless constant. When $\alpha_0 (\sigma - \sigma_0)/G < 0.8$, Eq. [8] reduces to Eq. [7a], *i.e.*, to a power law. On the other hand, in the high strain-rate regime, where $\sigma_0 \ll \sigma$, Eq. [8] is substantially equivalent to Eq. [4a].

V. CASES STUDIES: THE 6061 + 20 pct Al_2O_3 COMPOSITE PRODUCED BY INGOT METALLURGY AND THE 2014 PM ALLOY

A. *The 6061 + 20 pct Al_2O_3 composite*

Use of Eq. [8] requires accurate calculation of the threshold stress; this is normally impossible if only high strain-rate data are available, but this is not the case of the 6061 composite reinforced by 20 pct Al_2O_3, which has been investigated in torsion[63] and in shear creep.[54] Li and Langdon[54] carefully estimated the threshold stresses at 350 °C, 400 °C, and 500 °C; these values can be used to plot strain rate as a function of effective stress (Figure 9). As anticipated by Li and Langdon, inclusion of the high strain-rate data in the analysis confirms that there are two regimes: a low-stress

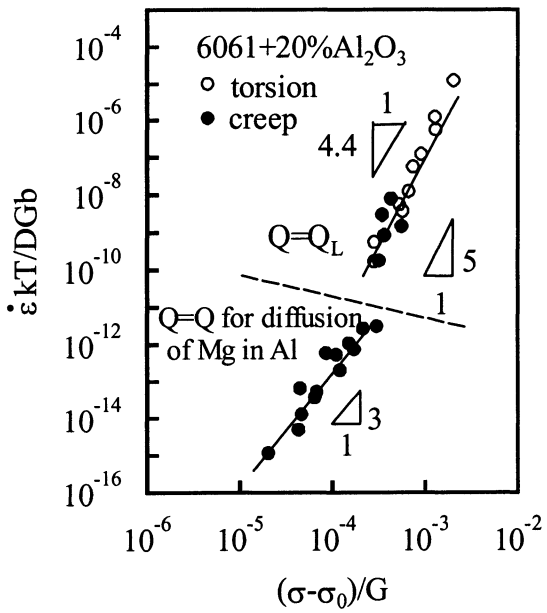

Fig. 10—Temperature-normalized minimum creep rate as a function of modulus-compensated effective stress for the the 6061 + 20 pct Al_2O_3 tested in torsion[64] and shear.[54]

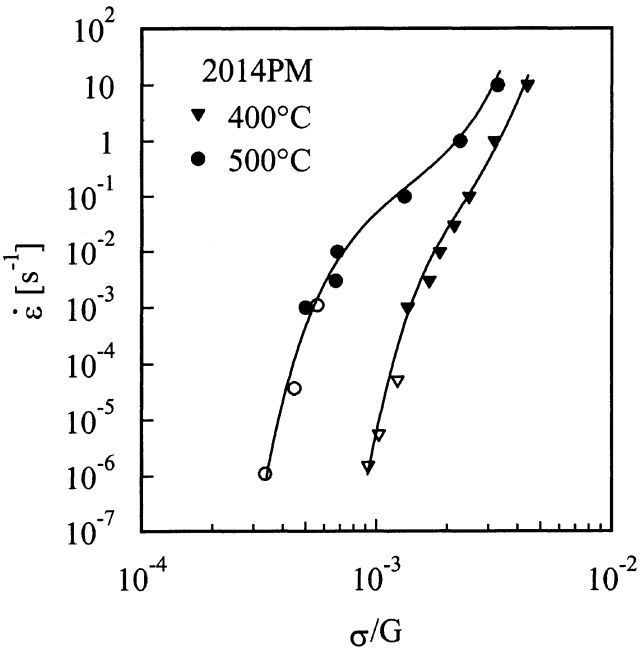

Fig. 11—Strain rate (or minimum creep rate) as a function of applied (or peak) stress for the 2014PM alloy tested at 400 °C and 500 °C.

regime, where viscous glide is the rate-controlling mechanism, and a high strain-rate regime, where climb is the rate-controlling mechanism. Since both mechanisms have similar activation energies (135 and 143 kJ mol^{-1}, respectively),[69,74] the temperature-normalized creep rate as a function of modulus-compensated effective stress of both regimes can conveniently be presented in the same plot (Figure 10).[63]

B. *The 2014PM alloy*

The preliminary successful application of the model to data from the literature suggested that a new set of data could be produced to test the model with another material, characterized by the presence of a threshold stress, *i.e.*, an unreinforced alloy produced by PM. To this end, the data obtained testing the 2014PM alloy (Figure 5) were completed by additional creep results at 500 °C and 450 °C. As in the torsioned samples, the material was solution-treated and stabilized, directly in the testing furnace in this case, for 24 hours at the testing temperature. The applied stress was selected to obtain short test duration, thus avoiding dynamic precipitation during creep (a behavior observed in the 2024PM alloy at 300 °C and 330 °C for sufficiently long creep exposure).[75,76] For the same reason, *i.e.*, to reduce any residual supersaturation of alloying elements, the testing temperature was high (at 400 °C and 500 °C the amount of precipitation during testing, after 24 hours stabilization, can reasonably be expected to be minimal).

Figure 11, where the stress (applied stress or peak stress) is plotted as a function of strain rate (minimum strain rate or testing strain rate) at 400 °C and 500 °C, reveals, as expected, a thresholdlike behavior. Details of the calculation of threshold stresses are given elsewhere.[77] However, it can be observed (Table I) that the values of threshold stress are a fraction (close to 15 pct) of the Orowan stress calculated on the basis of particle size and distribution. At 500 °C, Cu and Mg are in solid solution; as a result, the observed particles are, predictably, Al_2O_3 introduced during PM production route. At lower temperature, Cu and Mg precipitate during the 24 hour-stabilization treatment in form of Al_2Cu and Al_2CuMg, increasing the volume fraction of dispersed phases; this additional precipitation in turn raises Orowan and threshold stresses.

Table I. Threshold and Orowan Stresses Calculated on the Basis of Size and Volume Fraction of Dispersed Particles in the 2014 PM Alloy (Samples Torsioned at 10^{-3} and 1 s^{-1} at Each Temperature Was Analyzed); the Particle Size and Distribution Was Only Marginally Affected by the Difference in Strain Rate

Alloy	T (K)	σ_{Or} (MPa)	σ_0 (MPa)	σ_0/σ_{Or}
2014PM	573	144	21.1	0.15
	673	107	17.1	0.16
	773	59	7.0	0.12

When the temperature-normalized creep rate is plotted as a function of modulus-compensated effective stress (Figure 12), the experimental data again fall on two different curves. For simplicity, also in this case, the difference between activation energy for self-diffusion and activation energy for diffusion of Mg or Cu in the matrix has been neglected. In the low-stress regime, the strain-rate dependence on applied stress can be described by means of Eq. [8] with $n = 3$ (*i.e.*, viscous glide is the rate-controlling mechanism). In the high-stress regime, the data fall on a curve well described by Eq. [8] with $n' = 4.4$ and $\alpha_0 = 600$ (*i.e.*, plasticity is controlled by climb).

VI. IMPLICATIONS FOR THE DYNAMIC MATERIAL MODEL: EFFICIENCY OF THE POWER-DISSIPATION MAP

As mentioned previously, the dynamic material model has been used to predict the optimum forming conditions of both

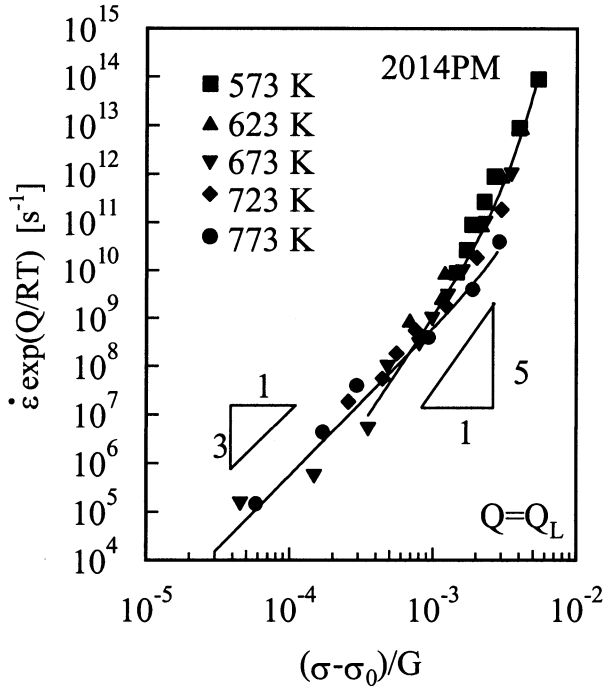

Fig. 12—Temperature normalized strain rate as a function of modulus compensated effective stress for the 2014PM alloy.

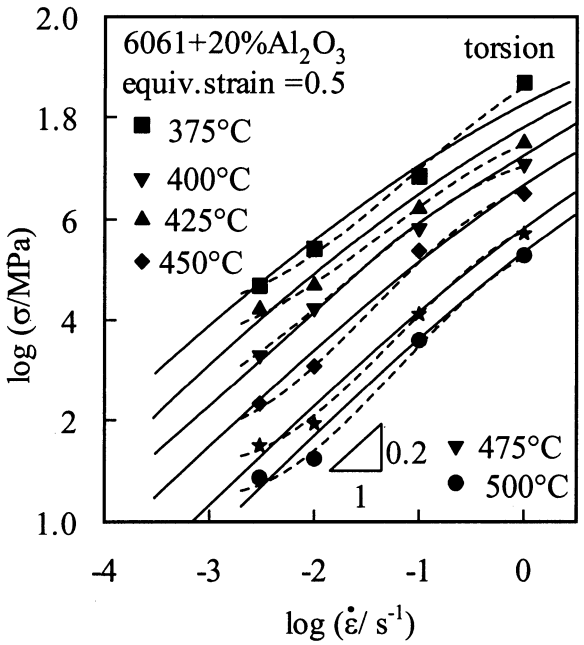

Fig. 13—Plot used for the *m* calculation (6061 − 20 pct Al_2O_3 in torsion, *i.e.*, same data of Fig. 7, replotted in different form). The broken lines represent the cubic splines of the data, the solid lines the curves obtained from constitutive equation (Eq. [8]).

composites and PM alloys, *i.e.*, of materials characterized by the existence of a threshold stress. In all the cases illustrated in Reference 28, the efficiency of power dissipation was calculated by plotting log σ *vs* log strain rate at constant temperature and strain and by interpolating these data by a third order polynomial equation (Figure 13). The same approach was followed in Reference 78 to obtain the power-efficiency dissipation map for the 6061 + 20 pct Al_2O_3

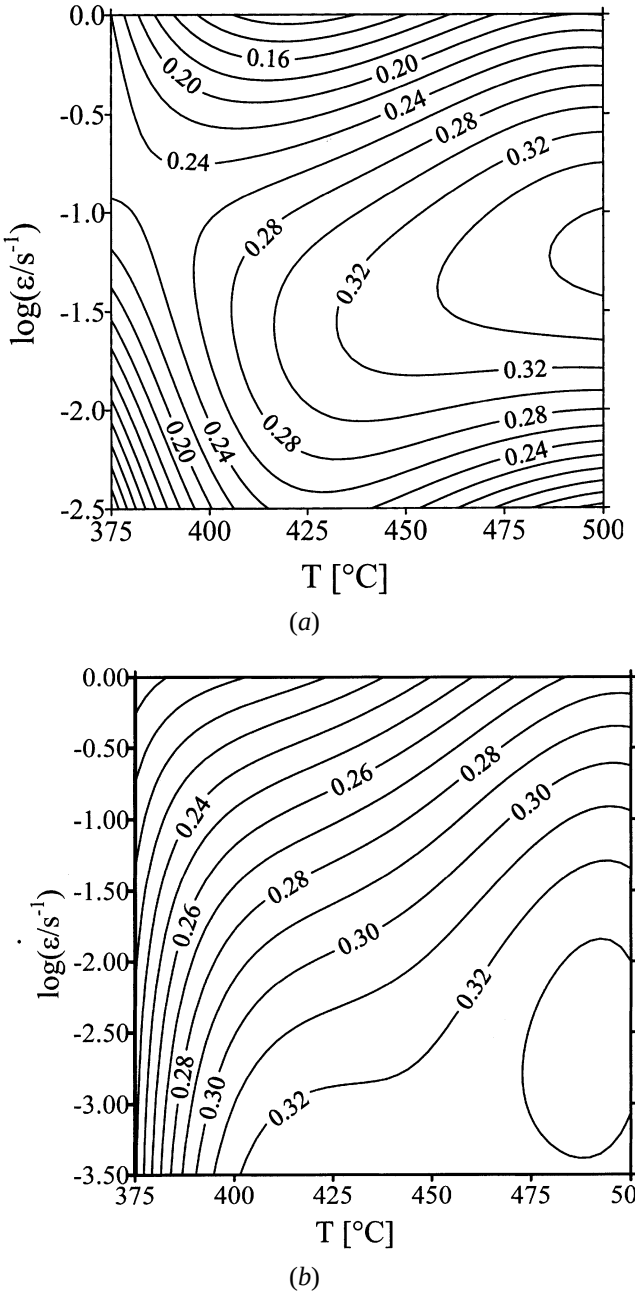

Fig. 14—(*a*) Power-efficiency dissipation map (the curves in the map represent iso-efficiency lines) obtained calculating *m* from the curves in Fig. 13; (a) broken lines, polynomial regression. (*b*) Power-efficiency dissipation map (the curves in the map represent iso-efficiency lines) obtained calculating *m* from the curves in Fig. 13; (b) solid lines, constitutive equation.

composite. It is quite obvious that this conventional approach in principle permits a precise description of the trend of experimental data; on the other hand, it is dramatically subject to any experimental scatter. For this reason, in the opinion of the authors of the present study, the approach based on recalculation of the maps directly from constitutive equations is superior to the conventional procedure based on a simple polynomial equation. The disadvantage, in the case of composites and complex alloys produced by PM, is that the constitutive equation, *i.e.*, Eq. [8], requires the estimation of threshold stress. This can be done for the 6061 + 20 pct Al_2O_3 by interpolating the σ_0 data obtained by Li and

Langdon.[54] Figure 13 presents the curves obtained from Eq. [8] following this procedure (solid lines) alongside the polynomial equations fitting the data (broken curves). Figure 14 plots the corresponding power-efficiency dissipation map. Comparison between the two maps in Figure 14 and those reported in Reference 28 clearly indicates that when the map is obtained on the basis of a constitutive equation, it lacks many of the "hills" and "valleys" that are frequently used to identify different regimes of deformation.[28]

VII. CONCLUSIONS

The conventional procedure for studying the high-temperature plasticity of Al-matrix composites and complex alloys produced by PM was analyzed. It was concluded that the plasticity of these materials, which generally exhibit a thresholdlike behavior when tested in a regime of conveniently low strain rates (*i.e.*, in creep conditions), can successfully be described by a modified form of the sinh constitutive equation that relates strain rate, flow stress, and temperature. In this equation, the simple substitution of flow stress with effective stress, *i.e.*, with the difference between flow stress and threshold stress, allows one to obtain a unified description of both high and low strain-rate plasticity. This procedure obviously requires the accurate determination of threshold stress, which can only be obtained by means of creep tests. The model can be further implemented by using the constitutive equation to determine the power-efficiency dissipation map, thus reconciling two separate approaches (the calculation of the constitutive equation and its correlation with ductility, and the procedure based on the dynamic material model).

ACKNOWLEDGMENTS

The research was supported by CNR, Progetto Finalizzato Materiali Avanzati/Materiali Compositi per applicazioni Strutturali and by Ministry of University and Scientific Research.

REFERENCES

1. H.J. McQueen and J.J. Jonas: in *Metal Forming: Interrelation between Theory and Practice*, A.L. Hoffmanner, ed., Plenum Publ. Corp., New York, NY, 1971, pp. 393-428.
2. H.J. McQueen and J.J. Jonas: *Man. Eng. Trans. (SME)*, 1973, vol. 2, pp. 209-33.
3. H.J. McQueen, E. Evangelista, N. Jin, and M.E. Kassner: *Metall. Mater. Trans. A*, 1995, vol. 26A, pp. 1757-66.
4. H.J. McQueen, E. Evangelista, and M.E. Kassner: *Z. Metallkd.*, 1995, vol. 82, pp. 336-45.
5. E. Evangelista, F. Gabrielli, P. Mengucci, and E. Quadrini: in *Strength of Metals and Alloys*, P.O. Kettunen, T.K. Lepisto, and M.E. Lehtonen, eds., Pergamon Press, Oxford, United Kingdom, 1988, pp. 977-82.
6. E. Cerri, E. Evangelista, A. Forcellese, P. Fiorini and J. Stobrawa: in *Strength of Metals and Alloys*, H. Oikawa *et al.*, eds., The Japan Institute of Metals, Tokyo, 1994, pp. 807-10.
7. E. Evangelista, E. DiRusso, H.J. McQueen, and P. Mengucci: in *Homogeneization and Annealing of Aluminum and Copper Alloys*, H.D. Merchant, J. Crane, and E.H. Chia, eds., TMS, Warrendale, PA, 1988, pp. 209-26.
8. H.J. McQueen: in *Hot Deformation of Aluminum Alloys*, T.G. Langdon, H.D. Merchant, J.G. Morris, and M.A. Zaidi, eds., TMS, Warrendale, PA, 1991, pp. 31-52.
9. H.J. McQueen: in *Hot Deformation of Aluminum Alloys*, T.G. Langdon, H.D. Merchant, J.G. Morris, and M.A. Zaidi, eds., TMS, Warrendale, PA, 1991, pp. 105-20.
10. H.J. McQueen and K. Conrad: in *Microstructural Control in Al. Alloy Processing*, H. Chin and H.J. McQueen, eds., TMS-AIME, Warrendale, PA, 1986, pp. 197-219.
11. E. Evangelista, A. Forcellese, F. Gabrielli, and P. Mengucci: in *Hot Deformation of Aluminum Alloys*, T.G. Langdon, H.D. Merchant, J.G. Morris, and M.A. Zaidi, eds., TMS, Warrendale, PA, 1991, pp. 121-39.
12. E. Evangelista, H.J. McQueen, and E. Cerri: in *Modelling of Plastic Deformation and Its Engineering Applications*, S.I. Andersen *et al.*, eds., Risø National Laboratory, Roskilde, Denmark, 1992, pp. 265-70.
13. L. Blaz and E. Evangelista: *Mater. Sci. Eng.*, 1996, vol. A207, pp. 195-201.
14. E.V. Konopleva, H.J. McQueen, and E. Evangelista: *Mater. Characterization*, 1995, vol. 34, pp. 251-64.
15. M.E. Kassner, J. Pollard, E. Evangelista, and E. Cerri: *Acta Metall. Mater.*, 1994, vol. 42, pp. 3223-30.
16. E. Cerri, E. Evangelista, A. Forcellese, and H.J. McQueen: *Mater. Sci. Eng.*, 1995, vol. A197, pp. 181-98.
17. H.J. McQueen and J.J. Jonas: in *Plastic Deformation of Materials*, R.J. Arsenault, ed., Academic Press, New York, NY, 1975, vol. 6, pp. 393-493.
18. D.J. Lloyd: *Int. Mater. Rev.*, 1994, vol. 39, pp. 1-23.
19. J.R. Pickens, T.J. Langan, R.O. England, and M. Liebson: *Metall. Trans. A*, 1987, vol. 18A, pp. 303-12.
20. X. Xia, P. Sakaris, and H.J. McQueen: *Mater. Sci. Technol.*, 1994, vol. 10, pp. 487-96.
21. X. Xia, H.J. McQueen, and P. Sakaris: *Scripta Metall. Mater.*, 1995, vol. 32, pp. 1185-90.
22. D. Yu and T. Chandra: in *Advanced Composites '93*, T. Chandra and A.K. Dhingra, eds., TMS, Warrendale, PA, 1993, pp. 1070-77.
23. H.J. McQueen, P. Sakaris, and J. Bowles: in *Advanced Composites '93*, T. Chandra and A.K. Dhingra, eds., TMS, Warrendale, PA, 1993, pp. 1193-98.
24. A. Alunni, E. Cerri, E. Evangelista, and A. Forcellese: in *Advanced Composites '93*, T. Chandra and A.K. Dhingra, eds., TMS, Warrendale, PA, 1993, pp. 1079-85.
25. H.J. McQueen, E.V. Konopleva, M. Myshlyaev, and Q. Qin: *Proc. 10th Int. Conf. on Composite Materials*, A. Poursartip and K. Street, eds., Woodhead Publ. Ltd, Cambridge, United Kingdom, 1995, vol. 2, pp. 423-30.
26. R. Raj: *Metall. Trans. A*, 1981, vol. 12A, pp. 1089-97.
27. Y.V.R.K. Prasad: *Ind. J. Technol.*, 1990, vol. 28, pp. 435-51.
28. Y.V.R.K. Prasad and S. Sasidhara: *Hot Working Guide: A Compendium of Processing Maps*, ASM INTERNATIONAL, Metals Park, OH, 1999.
29. B.V. Radhakrishna Bhat, Y.R. Mahajan, H.M. Roshan, and Y.V.R.K. Prasad: *Mater. Sci. Technol.*, 1995, vol. 11, pp. 167-73.
30. B.V. Radhakrishna Bhat, Y.R. Mahajan, and Y.V.R.K. Prasad: *Metall. Mater. Trans. A*, 2000, vol. 31A, pp. 629-39.
31. A. Forcellese, F. Gabrielli, S.M. Roberts, and P.J. Withers: *Proc. 11th Int. Conference on Composite Materials*, Melbourne, Victoria, Australia, M.L. Scott, ed., Australian Composite Structures Society-Woodhead Publ. Ltd., 1997, vol. III, pp. 143-53.
32. Y. Wang: *Mater. Sci. Eng.*, 1996, vol. A212, pp. 178-81.
33. K. Kucharova, A. Orlova, H. Oikawa, and J. Cadek: *Mater. Sci. Eng.*, 1988, vol. A102, pp. 201-09.
34. R.S. Mishra and A.B. Pandey: *Metall. Trans. A*, 1990, vol. 21A, pp. 2089-90.
35. K.-T. Park, E.J. Lavernia, and F.A. Mohamed: *Acta Metall. Mater.*, 1990, vol. 38, pp. 2149-59.
36. F.A. Mohamed, K.-T. Park, and E.J. Lavernia: *Mater. Sci. Eng.*, 1992, vol. A150, pp. 21-35.
37. A.B. Pandey, R.S. Mishra, and Y.R. Mahajan: *Acta Metall. Mater.*, 1992, vol. 40, pp. 2045-52.
38. G. Gonzalez-Doncel and O.D. Sherby: *Acta Metall. Mater.*, 1993, vol. 41, pp. 2797-2805.
39. K.-T. Park and F.A. Mohamed: *Metall. Mater. Trans. A*, 1995, vol. 26A, pp. 3119-30.
40. J. Cadek, V. Sustek, and M. Pahutova: *Mater. Sci. Eng.*, 1994, vol. A174, pp. 141-47.
41. J. Cadek, H. Oikawa, and V. Sustek: *Mater. Sci. Eng.*, 1995, vol. A190, pp. 9-23.
42. J. Cadek, M. Pahutova, and V. Sustek: *Mater. Sci. Eng.*, 1998, vol. A246, pp. 252-68.
43. J. Cadek, K. Kucharova, and V. Sustek: *Scripta Mater.*, 1999, vol. 40, pp. 1269-75.

44. J. Cadek, K. Kucharova, and S.J. Zhu: *Mater. Sci. Eng.*, 2000, vol. A281, pp. 162-68.
45. J. Cadek, K. Kucharova, and S.J. Zhu: *Mater. Sci. Eng.*, 2000, vol. A283, pp. 172-80.
46. J. Cadek, K. Kucharova, and S.J. Zhu: *Mater. Sci. Eng.*, 2001, vol. A297, pp. 176-84.
47. S.J. Zhu, L.M. Peng, Q. Zhou, Z.Y. Ma, K. Kucharova, and J. Cadek: *Mater. Sci. Eng.*, 2000, vol. A282, pp. 273-84.
48. Z.Y. Ma and S.C. Tjong: *Mater. Sci. Eng.*, 2000, vol. A278, pp. 5-15.
49. W.J. Kim, H. Yeon, D.H. Shin, and S.H. Hong: *Mater. Sci. Eng.*, 1999, vol. A269, pp. 142-51.
50. N. Matsuda, J. Akaike, K. Hongo, and K. Matsuura: *Mater. Sci. Eng.*, 1997, vols. A234–A236, pp. 751-54.
51. A.B. Pandey, R.S. Mishra, A.G. Paradkar, and Y.R. Mahajan: *Acta Mater.*, 1997, vol. 45, pp. 1297-1306.
52. Y. Li and F.A. Mohamed: *Acta Mater.*, 1997, vol. 45, pp. 4775-85.
53. Y. Li and T.G. Langdon: *Scripta Mater.*, 1997, vol. 36, pp. 1457-60.
54. Y. Li and T.G. Langdon: *Acta Mater.*, 1997, vol. 45, pp. 4797-4806.
55. Y. Li and T.G. Langdon: *Metall. Mater. Trans. A*, 1997, vol. 28A, pp. 1271-73.
56. Y. Ma and T.G. Langdon: *Mater. Sci. Eng.*, 1997, vol. A230, pp. 183-87.
57. Y. Li and T.G. Langdon: *Acta Mater.*, 1998, vol. 46, pp. 1143-55.
58. Y. Li and T.G. Langdon: *Acta Mater.*, 1998, vol. 46, pp. 3937-48.
59. Y. Li and T.G. Langdon: *Mater. Sci. Eng.*, 1998, vol. A245, pp. 1-9.
60. Y. Li and T.G. Langdon: *Metall. Trans. A*, 1998, vol. 29A, pp. 2523-31.
61. Y. Li and T.G. Langdon: *Acta Mater.*, 1999, vol. 47, pp. 3395-403.
62. F. Bardi, E. Evangelista, and S. Spigarelli: *Proc. 28° Convegno Nazionale AIM*, Associazione Nazionale Metallurgia, Milano, Italy, 2000, vol. II, pp. 853-62.
63. S. Spigarelli, E. Evangelista, E. Cerri, and T.G. Langdon: *Mater. Sci. Eng.*, in press.
64. E. Cerri, S. Spigarelli, E. Evangelista, and P. Cavaliere: *Mater. Sci. Eng.*, 2001, in press.
65. O.D. Sherby and P.M. Burke: *Progr. Mater. Sci.*, 1967, vol. 13, p. 325.
66. E. Evangelista, S. Spigarelli, F. Bardi, and Mira Vukcevic: *Proc. Int. Conf. EUROMAT 2001*, in press.
67. J. Sarkar, Y.V.R.K. Prasad, and M.K. Surappa: *J. Mater. Sci.*, 1995, vol. 30, p. 2483.
68. B.V. Radhakrishna Bhat, Y.R. Mahajan, H.M. Roshan, and Y.V.R.K. Prasad: *Mater. Sci. Eng.*, 1994, vol. A189, p. 137.
69. F.A. Mohamed and T.G. Langdon: *Metall. Trans.*, 1974, vol. 5, pp. 2339-45.
70. M.E. Kassner and M.-T. Prado: *Progr. Mater. Sci.*, 2000, vol. 45, pp. 1-43.
71. K.-T. Park, E.J. Lavernia, and F.H. Mohamed: *Acta Metall. Mater.*, 1994, vol. 42, pp. 667-78.
72. S. Spigarelli, M. Cabibbo, E. Evangelista, and T.G. Langdon: in *Creep and Fracture of Engineering Materials and Structures*, The Institute of Materials, London, 2001, pp. 271-80.
73. J. Friedel: *Dislocations*, Pergamon Press, Oxford, United Kingdom, 1964.
74. S.J. Rothman, N.L. Peterson, L.J. Nowicki, and L.C. Robinson: *Phys. Status Solidi (b)*, 1974, vol. 63, p. K29.
75. L. Kloc, E. Cerri, S. Spigarelli, E. Evangelista, and T.G. Langdon: *Mater. Sci. Eng.*, 1996, vol. A216, pp. 161-68.
76. L. Kloc, S. Spigarelli, E. Cerri, E. Evangelista, and T.G. Langdon: *Acta Mater.*, 1997, vol. 45, pp. 529-40.
77. F. Bardi, M. Cabibbo, S. Spigarelli, and E. Evangelista: University of Ancona, unpublished research.
78. F. Bardi, M. Cabibbo, S. Spigarelli, and E. Evangelista: *Mater. Sci. Eng.*, in press.